

---

# A Reinforcement Learning Based Universal Sequence Design for Polar Codes

---

David Kin Wai Ho<sup>1</sup> Arman Fazeli<sup>2</sup> Mohamad M. Mansour<sup>2</sup> Louay M. A. Jalloul<sup>2</sup>

## Abstract

To advance Polar code design for 6G applications, we develop a reinforcement learning-based universal sequence design framework that is extensible and adaptable to diverse channel conditions and decoding strategies. Crucially, our method scales to code lengths up to 2048, making it suitable for use in standardization. Across all  $(N, K)$  configurations supported in 5G, our approach achieves competitive performance relative to the NR sequence adopted in 5G and yields up to a 0.2 dB gain over the beta-expansion baseline at  $N = 2048$ . We further highlight the key elements that enabled learning at scale: (i) incorporation of physical law constrained learning grounded in the universal partial order property of Polar codes, (ii) exploitation of the weak long term influence of decisions to limit lookahead evaluation, and (iii) joint multi-configuration optimization to increase learning efficiency.

## 1. Introduction

### 1.1. Polar Codes in 5G NR and beyond

Polar codes are an essential component of the 5G NR standard, responsible for ensuring the integrity of uplink control information (UCI) transmitted over the physical uplink control channel (PUCCH) and the physical uplink shared channel (PUSCH) in the uplink. Similarly in the downlink, Polar codes protect the integrity of downlink control information (DCI) transmitted over the physical downlink control channel (PDCCH), as well as the master information block (MIB) transmitted over the physical broadcast channel (PBCH).

As the industry moves towards 6G, there is an anticipated demand for larger DCI payloads to support additional features,

<sup>1</sup>Apple, San Diego, USA <sup>2</sup>Apple, Sunnyvale, USA. Correspondence to: David Ho <davidkwho@apple.com>.

*Proceedings of the 43<sup>rd</sup> International Conference on Machine Learning*, Seoul, South Korea. PMLR 306, 2026. Copyright 2026 by the author(s).

increased channel state information feedback and other signaling needs. In addition, stronger error protection will be necessary to enhance cell-edge user experience. The Polar codes and the associated universal sequence defined in 5G NR (Bioglio et al., 2020) are currently limited to a block length of 1024 bits. This restricts the maximum payload size and the number of parity bits available for improved protection under poor channel conditions. For large payloads, the current 5G NR strategy segments the data across multiple, smaller code blocks; however, these smaller codes cannot exploit the additional polarization layers available at larger block lengths. For enhanced protection, the standard resorts to suboptimal repetition coding. Extending Polar code lengths can unlock performance gains unattainable in the current specification.

For a Polar code to function optimally under successive cancellation list (SCL) decoding, the information bits must be assigned to the synthetic channels in a way that minimizes the overall error probability. As an example, consider a  $(128, 36)$  Polar code with code length  $N = 128$  bits and payload size  $K = 36$  bits. Of the 128 synthetic channels, one must define a mapping to optimally assign the 36 payload bits and freeze the remaining bit channels by setting the input to zero. The resultant mapping, referred to as a frozen bitmap, must be specified for each  $(N, K)$  configuration supported by the standard. Given the large variability of channel conditions and physical resource constraints in a multi-user wireless environment, a wide range of code lengths and all possible code rates (defined by  $CR = K/N$ ) must be supported. The 5G NR standard supports  $N \in \{32, 64, 128, 256, 512, 1024\}$  and  $K = 12$  and up to the number of physically transmitted bits.

Polar codes share the same Kronecker product construction as Reed-Muller (RM) codes (Reed, 1954; Muller, 1954); however, their bit channel selection mechanism and optimizing objective are markedly different. In RM codes, the rows of the generator matrix are selected based on the largest Hamming weights, yielding a channel independent design that maximizes minimum distance, which is a desirable property for short codes. In contrast, Polar codes select rows by maximizing conditional mutual information (or equivalently, minimizing the Bhattacharyya parameter), re-

sulting in a channel-specific design that minimizes the error probability under successive cancellation (SC) decoding. Invented by Arikan in 2009 (Arikan, 2009), Polar codes is the first channel code with an explicit construction that provably achieves the channel capacity. In practice, Polar codes offers superior performance with low-complexity decoding algorithms, making them indispensable for 5G control channels where they outperform LDPC codes at short block lengths. We refer interested readers to this excellent introduction to Polar codes.<sup>1</sup>

## 1.2. Adoption of universal reliability sequence

The sheer number of possible bit mappings presents a significant challenge for storage requirements and computational burden if they are generated on demand. However, if the problem can be simplified such that each synthetic channel is associated with a reliability metric and these channels be ranked universally by this metric for all block lengths, then the problem reduces to designing a single universally applicable sequence for all  $(N, K)$  combinations. For each  $(N, K)$ , the assignment method reduces to finding all channel indices less than  $N$  and selecting out of this set the  $K$  most reliable indices to carry the information bits. Only a single maximum length  $N$  sequence is stored in memory, substantially reducing both storage and computational complexity. This universal sequence approach has been adopted in the 5G NR standard (Bioglio et al., 2020).

## 1.3. Reinforcement learning in code construction

Noting that existing code construction methods do not produce optimal codes for Polar SCL decoding, (Liao et al., 2021) began the exploration of using reinforcement learning to learn the bit assignment directly from the outcome of a Polar SCL decoder. This early approach used a Tabular RL method (SARSA) to learn the frozen bit assignment for a fixed payload size, a fixed code length and a fixed signal-to-noise ratio (SNR). Because tabular RL lacks generalization capability across code configurations, this method is not scalable to a large number of codes. In mobile communication systems, the dynamic and wide ranging fading environments requires operations over diverse code rates, code lengths and SNR regimes. Similar attempts by (Mishra et al., 2022) approached the PAC code construction problem using a modified Q-learning algorithm, which inherits the same limitations of Tabular RL. Moreover, their use of the Reed-Muller initialization rule severely limits the algorithm's ability to learn optimal assignments. As shown experimentally, the RM rule becomes highly suboptimal at moderate code lengths. To address the scalability limitations of Tabular methods, (Liao et al., 2023) applied a deep-RL approach based on Deep Q-learning with a graph neural

network (GNN) approximating the action-value function. The algorithm utilized a heterogeneous-GNN, where predicted values are refined through multiple stages of message passing among graph nodes. Our approach was inspired by this powerful deep reinforcement learning technique and the promise of scalability of this work, although we note that the training complexity of the proposed method limited its use to short code lengths.

## 1.4. Universal Partial Order

Building upon Arikan's foundational work, researchers discovered the universal partial order (UPO), a set of relations that governs the reliability among the synthetic bit channels and remains valid irrespective of the underlying physical channel characteristics under the assumption of SC decoding (Schürch, 2016). (He et al., 2017) exploited the UPO relations to develop an efficient sequence construction scheme based on beta-expansion theory. Subsequent studies (Yao et al., 2024; Liu et al., 2024) extended this line of research by discovering new partial order relations that enable improved performance for sequentially rate-matched Polar codes.

## 1.5. Physical law constrained machine learning

Many problems in material sciences and physics concern the learning of phenomena and the generation of entities that adhere to known geometric structure or physical laws. While an ML agent may learn the distribution of the training data with a high degree of accuracy, it might struggle to generate novel samples that exhibit specific desired properties, particularly when such samples are underrepresented or absent in the dataset. However, because of the enormous space involved, a guided strategy is needed to constrain the agent to generate samples within the distribution of interest. This motivated (Okabe et al., 2025) to incorporate geometric constraints in the SCIGEN model, thereby improving the quality of generated samples. In physics, even with abundant observational data, purely data-driven models often produce predictions that are physically inconsistent or implausible. Therefore, it is essential that fundamental physical laws and domain knowledge be incorporated in the model as an informative prior. Physics-informed learning (Karniadakis et al., 2021) advocates the inclusion of physical laws based constraints either as inductive bias (implemented as hard constraints) or as learning bias (implemented as penalty terms). This approach enhances generalization in the small data regime by restricting deep learning models to operate in lower-dimensional manifolds consistent with theory. Guided by this principle, we leverage the known UPO relations that govern the relative reliability of the synthetic channels to improve the predictive performance of the RL agent while keeping the data demand modest.

<sup>1</sup>Polar codes tutorial from Prof. Balatsoukas-Stimming

## 1.6. Contributions

We present the first openly-documented RL-based universal sequence design method that is scalable to any code lengths, trainable within reasonable time budgets using standard GPU/CPU compute infrastructure, and adaptable to any channel conditions and decoding strategies. Our approach integrates a deep reinforcement learning method, specifically Proximal Policy Optimization (PPO) (Schulman et al., 2017) to eliminate the need for an experience replay buffer and improve training stability, constrains the search space using the UPO relations to make the optimization task tractable, embeds lower-N sequences to preserve the optimality of performance across smaller block lengths, adopts a Monte-Carlo-Tree-Search (MCTS) inspired iterative learning strategy to limit lookahead evaluation, and applies progressive constraint relaxation to improve the quality of the result. Moreover, we introduce a joint optimization framework that promotes knowledge transfer among different configurations, significantly improving learning efficiency. Our method achieves competitive performance across all  $(N, K)$  configurations supported in 5G NR relative to the NR sequence and delivers up to 0.2 dB gain over beta-expansion at  $N = 2048$ . Source code is available at <https://github.com/apple/ml-rl-universal-sequence-design>.

## 2. Problem Definition

Given a propagation channel environment and a Polar decoding algorithm, with limits  $N_{max}$ ,  $N_{min}$  and  $K_{min}$ , we seek to find an optimal stochastic policy where the sampled instances produce, with high probability, an absolute ordering (the universal sequence) that outperforms the beta-expansion algorithm (baseline) in terms of block error rate (BLER)<sup>2</sup> over all permissible block length, payload combinations, i.e. for all  $(N, K)$  Polar codes derived using the absolute ordering, where  $K_{min} \leq K < N$ ,  $N_{min} \leq N \leq N_{max}$  ( $N$  must be an integer power of 2).

A subtle but important aspect of the problem is that bit indices participate in the frozen bitmaps of codes from multiple block lengths. Thus effectively we have a multi-objective optimization problem without a unique dominant winner. To resolve this ambiguity, we explicitly prioritize the performance at smaller block lengths over larger ones.

In addition to achieving the main objective, the proposed method must be computationally scalable to practical block lengths (up to  $N_{max} = 2048$ ), trainable within a reasonable time budget. Scalability remains a major challenge for existing RL-based approaches.

<sup>2</sup>In practice the relative BLER performance is measured as the SNR gap between two schemes at some fixed BLER e.g. 0.01.

## 3. Proposed Method

### 3.1. High level description

We first provide a high-level overview of the construction method before detailing each step. The sequence is constructed in a nested, iterative manner, starting from  $N = N_{min}$ . The sequence generated at each stage serves as a sub-sequence that is embedded within the next length progression  $N_{next} = 2N$ . This ensures that the performance at the current  $N$  is preserved. At each step, an RL-based neural-assisted search is conducted to identify a candidate sequence that jointly maximizes the performance of all length- $N$  polar codes. It is important to note that due of the universal reliability ranking, for any fixed  $N$ , the first  $J$  bit channel decisions influence the performance of  $(N, K)$  Polar codes for all  $K > J$ . The UPO property of Polar codes is exploited to constrain the search space, keeping the optimization computationally feasible. Two additional relaxation techniques are incorporated to expand the search space selectively, allowing the discovery of higher-performing candidates.

### 3.2. Action space constraint management

To scale the proposed approach to  $N_{max} = 2048$  (denoted N2048), it is critical to adopt a principled method of restricting the search space, without which the search becomes computationally intractable. Using UPO, we reduced the state space for N2048 from  $10^{5894}$  to  $10^{2582}$ . In addition, without any knowledge of the previous lower-N result, the current  $N$  search will produce a suboptimal sequence at lower-N. Thus, it is essential that we enforce the ordering of indices in the lower-N search, which preserves the performance at lower-N. We refer to this technique as *lower-N embedding*. However, we found empirically that lower-N embedding leads to degradation in performance at large block-lengths. From in-depth analysis at  $N$ , the preferred ordering of the initial portion of the lower-N indices  $i \in \{j \mid j < N_{lower}\}$  is observed to deviate from that of the lower-N sequence. Because the standard defines a minimum payload size for UCI/DCI, we exploit this by relaxing the constraint of the first  $K_{min}$  imposed by the lower-N sequence, since the relative ordering of these bits do not influence the performance at  $N_{lower}$ . Thus we introduce this as the first relaxation step. Second, since UPO is derived under the assumption of SC decoding rather than SCL decoding, relaxing the UPO constraint can expose high-performing candidates under SCL decoding. In addition to the immediate neighbors in the UPO lattice, we extend the action space to include one-hop neighbor nodes that would normally violate UPO consistency through the process of *node promotion*. We refer to the combined constraints as the *UPO+ rule*. Figure 1 illustrates this concept.

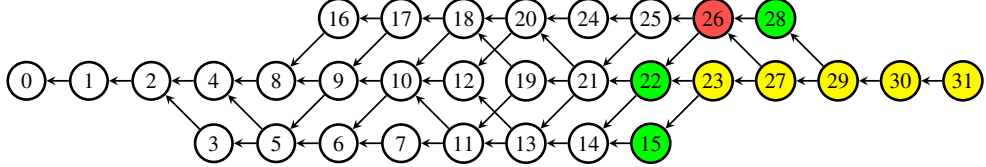


Figure 1. UPO lattice with the current context in yellow, the immediate neighborhood in green and the disallowed neighbor in red. Our proposed relaxation will include the red node as permissible action in the current context, as this is the immediate neighbor of node 27.

### 3.3. Universal partial order

We restate the universal partial order result here for convenience.

**Definition 3.1.** A synthetic channel  $i$  is more reliable than  $j$  as measured by the mutual information or equivalently the Bhattacharyya parameter (Arikan, 2009), is denoted  $i \succ j$ .

Given any pair of synthetic channel indices  $(x, y)$ , their reliability relation is determined by the following rules (Mondelli et al., 2018):

- **Addition:** If a binary representation of the index of a synthetic channel is  $(a, b, 0, c)$ , then it must be less reliable than the synthetic channel whose index has the binary representation  $(a, b, 1, c)$ . This relation holds for one or more consecutive bits. For example:

$$\begin{aligned} 4(1, 0, 0) &\prec 5(1, 0, \underline{1}), \\ 9(1, 0, \underline{0}, 1) &\prec 15(1, \underline{1}, 1, 1). \end{aligned}$$

- **Left-swap:** If a binary representation of the index of a synthetic channel is  $(a, 0, b, 1, c)$ , then it must be less reliable than the synthetic channel whose index has a binary representation  $(a, 1, b, 0, c)$ . This pattern can appear multiple times, and the 0, 1 pair do not need to be adjacent to each other. For example:

$$\begin{aligned} 3(\underline{0}, \underline{1}, 1) &\prec 5(\underline{1}, \underline{0}, 1), \\ 13(\underline{0}, 1, \underline{1}, 0, 1) &\prec 25(\underline{1}, 1, \underline{0}, 0, 1). \end{aligned}$$

The nested and symmetric property of UPO leads to an efficient recursive construction of these relations, as demonstrated in section II-B of (He et al., 2017). This structure forms the theoretical foundation upon which our constrained action mechanism is built.

### 3.4. Benefit of joint multi configuration optimization

Our approach of jointly optimizing a range of Polar code configurations represents a significant departure from prior learning based methods and is primarily motivated by the need to achieve learning efficiency at scale. Since the task of universal sequence design can be viewed as learning the

reliability ranking across synthetic channels, knowledge learned from smaller  $K$  configurations can be transferred to accelerate convergence for larger  $K$  cases. This leads to substantially higher learning efficiency while maintaining near optimal result.

The approach used in (Liao et al., 2023) limits training to a fixed  $(N, K)$  code and relies on the agent's ability to generalize to other code configurations. Since the agent has not seen the decoder behavior for shorter payload lengths, its performance degrades significantly in this regime. Even when tasked to generate frozen bitmaps for larger payload sizes, which are presented in training, the agent's generalization performance remains suboptimal, and additional fine-tuning is required to close the optimality gap. Consequently, these weaknesses hinder practical deployment of this approach for online bitmap generation.

*Remark 3.2.* It is a general observation that in physical layer communications applications, the high precision required often makes generalization to unseen scenarios suboptimal unless strong domain structure is explicitly encoded as inductive bias. A practical rule of thumb is to include the entire test distribution during training even when reward generation induces additional computational burden. Reward-generation efficiency is further discussed in Appendix C.

*Remark 3.3.* An alternative to full test distribution coverage is to encourage fast adaptation via the meta learning framework (Finn et al., 2017). This represents a promising direction for future investigation.

### 3.5. Restrict search with limited lookahead

For short block lengths, it is possible to evaluate the rewards for all  $K$ 's in the fixed length- $N$  family of Polar codes. However, as we move to larger block lengths, joint optimization of all  $K$ 's is no longer effective. This is largely due to the use of a summarizing scalar reward, like averaging over the BLER of all Polar codes. The current action selection attempts to differentiate between minute values; the ability to find the true optimal value is completely swamped by a large number of noisy estimates.

To mitigate this smoothing effect, we rely on the empirical

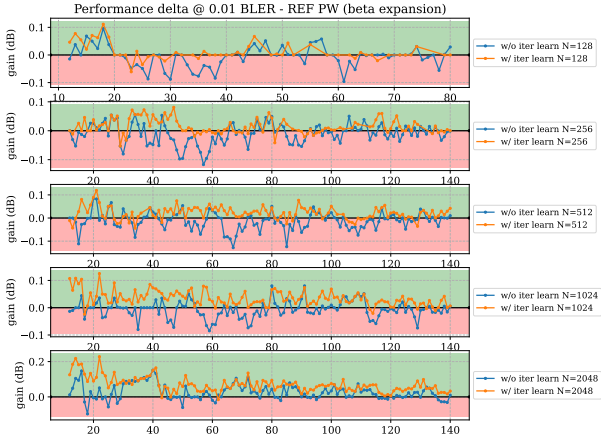


Figure 2. Performance impact of iterative learning in joint multi-configuration optimization.

### Algorithm 1 Neural-assisted sequence learning

```

function SUBSEQSEARCH( $s, s_l, I, W$ )
     $\triangleright$  Run UPO+-GNN-PPO
     $\pi \leftarrow \arg \max_{\pi} v_{\pi}(s; s_l, I + W)$   $\triangleright$  See (1)
     $s \leftarrow \text{greedy}(\pi|s)$ 
    return  $s$ 
end function

```

observation that the relative ordering of the indices will have little long range influence. In other words, the  $J$ -th decision will have only minor impact on the performance of a  $(N, K)$  code where  $K \gg J$ . Using this, we modify the learning procedure such that for each of the agent's decisions, we perform rollouts up to a fixed lookahead window length  $W$ . Once we have committed to these decisions, we will learn the next decision by sliding the lookahead window forward. This is reminiscent of a game playing agent where it has a limited budget to search for an advantageous move, and once it executes the move, it will then proceed to evaluate the next move based on the current board configuration. We call this approach *iterative learning*.

In Figure 2 we compare the performance of joint multi-configuration optimization with iterative learning using a lookahead window of 16 to an earlier approach where we attempt to learn 512 configurations simultaneously. The learned sequence with iterative learning achieves gains across almost all configurations while we see degradation in a significant number of configurations without iterative learning.

In the next section, we will explain in detail the deep reinforcement learning techniques adopted in this work.

### Algorithm 2 Nested iterative sequence construction

```

Require:  $N_{min}, N_{max}, K_{min}, W$ 
Initialize  $N \leftarrow N_{min}$ ,  $s_{lower} \leftarrow \emptyset$ ,
while  $N \leq N_{max}$  do
     $\triangleright$  Conduct search for a candidate sequence at  $N$ 
    Initialize  $K \leftarrow K_{min}$ , ranking  $r \leftarrow \emptyset$ 
    while  $K \leq N$  do
        if  $K = K_{min}$  then
             $\triangleright$  Search for the first  $K$  indices
             $s = \text{SUBSEQSEARCH}(\emptyset, s_{lower}, K, W)$ 
             $r \leftarrow r \cup s_{1:K}$ 
        else
             $\triangleright$  Search for the  $K$ -th index
             $s = \text{SUBSEQSEARCH}(r, s_{lower}, 1, W)$ 
             $r \leftarrow r \cup s_K$ 
        end if
         $K \leftarrow K + 1$ 
    end while
     $s_{lower} \leftarrow r$ 
     $N \leftarrow 2N$ 
end while
return  $r$ 

```

## 4. Deep reinforcement learning

In our RL formulation, the agent's objective is to rank bit indices from the most to the least reliable, selecting one index at each decision step. Each RL task operates on a fixed code length  $N$ . During each episode, the agent is provided with a payload size  $K$  and must output the  $K$  bit indices used for carrying information bits in the  $(N, K)$  code. The agent is rewarded based on a balance between the performance of the current code and that of all codes with larger payloads ( $K' > K$ ). The reward is issued only at the end of each episode, which corresponds to the negative BLER of the resulting code. The objective is thus to solve the following value-function maximization problem:

$$\pi_* = \arg \max_{\pi} v_{\pi}(s; s_l, W), \text{ for all } s \in \mathcal{S}, \quad (1)$$

$$v_{\pi}(s; s_l, W) = \mathbb{E}_{\pi(s, s_l), K}[-\log(\text{BLER}_{K, N})],$$

$$K \sim \text{Uniform}(K(s) : K_{max}), \quad (2)$$

where

1.  $s$  is the current state,  $s = (i_1, i_2, \dots, i_{K-1})$  for some  $K$ .
2.  $K(s)$  is the  $K$  as defined in 1.
3.  $K_{max} = \min(N, K + W)$ .
4.  $W$  is the lookahead window length.
5.  $\pi(s, s_l)$  is the stochastic policy, with frozen past actions  $s$  and constrained under the UPO+ rule with embedded lower- $N$  sequence  $s_l$ .

6.  $\text{BLER}_{K,N}$  is the block error rate of a  $(N, K)$  Polar code with information bits mapped to the current  $\pi(\mathbf{s}, \mathbf{s}_l)$  realization of bit indices.

#### 4.1. States

The observed state can be viewed as an injective mapping of the agent’s prior actions. We encode the state as a graph with nodes representing all synthetic bit channels, and setting the node type to selected or free  $\{\mathbf{S}, \mathbf{F}\}$  based on the agent’s actions. This ensures the Markovian property of the MDP problem is met. However, to reduce the message passing complexity over the graph, we confined the connections of nodes to a context window of past actions and the current action set. We have experimented with different context window size, i.e. the number of past actions to be considered in the policy network, and found that restricting the window to a small number of previous decisions was sufficient to maintain good performance. This truncation is reasonable given the observation of diminishing long-term influence of past decisions (Section 3.5).

#### 4.2. Actions

As detailed in Section 3.2, the set of permissible actions at any given state  $s$  is determined by the UPO+ rule – a composite constraint that combines the UPO relations, lower-N sequence enforcement, initial  $K_{min}$  index relaxation, and node promotion. The relationship between the state and its permissible actions is encoded in the state-action transition function  $A(s_{past}, s_{lower})$ , where  $s_{past}$  denotes the sequence of all past actions and  $s_{lower}$  is the lower-N sequence. This logic is precisely captured in the UPO class of the accompanying source code.

#### 4.3. Reward

The reward is defined as the negative log BLER of the  $(N, K)$ -Polar code produced by the policy at the end of each episode. The specific SNR for which the BLER is evaluated has a substantial impact on the value prediction of the actor-critic model. We anchor the SNR to the required SNR needed to achieve the target 1% BLER for the reference beta-expansion sequence. This choice ensures that the evaluation point remains close to the operating region of the optimal sequence, as the observed performance gap between beta-expansion and other SOTA sequences is less than 0.2 dB. We observe vastly improved value loss in the training compared to an alternate scheme using a constant capacity gap. This is defined as:

$$\text{SNR}_{\text{eval}, K, N} = 10 \log_{10}(2^R - 1) + \text{SNR}_{\text{offset}, N}, \quad (3)$$

where  $R = K/N$  is the code rate and SNR is in dB. In Fig-

ure 3, the capacity gap, defined by the separation between the theoretical achievable SNR of a code and the SNR obtained from beta expansion at 1% BLER, is plotted over all configurations. It reveals that the gap is not constant across all configurations. Thus a fixed capacity gap increases variance in value prediction at convergence and creates a reward bias toward better performing code configurations.

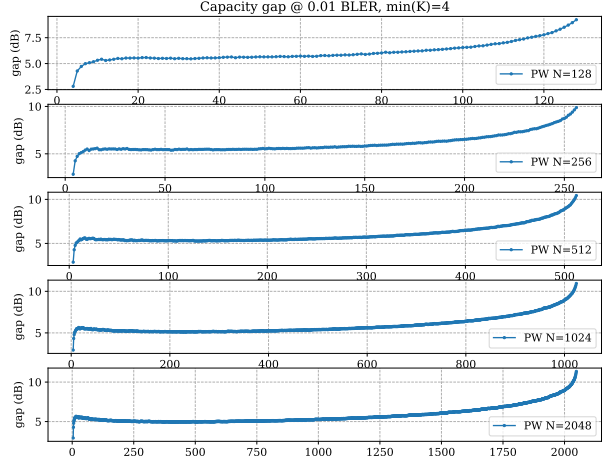


Figure 3. Required SNR characterization for baseline beta-expansion (PW) sequence used to define evaluation anchors.

The pseudo code of the iterative sequence construction method is given in Algorithms 1 and 2.

#### 4.4. RL algorithm

After extensive experimentation with DQN including many of its enhancements (Mnih et al., 2015; Hessel et al., 2018) and PPO (Schulman et al., 2017), we adopted PPO as the primary algorithm for all universal sequence learning tasks. We observed stability issues with DQN early on (at  $N = 256$ ), a substantial amount of effort was required to stabilize training. Furthermore, DQN’s reliance on an experience replay buffer introduces synchronization overhead when parallelizing across GPU processes. This substantially limits throughput and scalability.

In contrast, we found the stable-baseline3 implementation of PPO (Raffin et al., 2021) to be highly stable and robust across all tested configurations, requiring minimal hyperparameter tuning. Extensive sweeps over learning rate, clipping ratio, GAE lambda and entropy regularization confirmed that PPO’s performance remains largely insensitive to variations in these parameters. Additionally, PPO does not depend on a persistent replay buffer, it enables efficient data parallelism across compute nodes. This property proved critical for making N2048 training computationally feasible.

#### 4.5. Actor-Critic Model

The architecture of the actor-critic model is largely determined by the chosen state representation. In our design, we elected to use a graph to encode the context and the action space, where each node in the graph maps to a bit index in the context or a bit index in the permissible action space. A graph representation provides a general description of the relations between nodes and additional semantic relations can be incorporated *a priori* or learned through gating or attentional mechanisms.

First we construct a graph of all synthetic channels each represented as a node in the graph. However, not all nodes are connected. Only the current context and the action space are fully connected to each other. Nevertheless, all nodes participate in the model’s final decision.

Each node is assigned two input features. The first feature is a node type indicating whether the node has been selected (information carrying) or remains unselected (frozen). The second feature encodes the binary representation of the index itself, motivated by the observation that many theory-based selection schemes such as Reed-Muller and beta expansion are functions of the binary representation. An initial layer learns a type specific embedding and an embedding derived from the binary representation, which are combined using summation rather than concatenation – a choice that consistently yielded superior performance across trials.

The resulting embedding is passed to a stack of graph convolutional layers employing the GraphSAGE operator (Hamilton et al., 2017). We chose this operator because of its effectiveness and computational efficiency. We have experimented with many advanced gated (Bresson & Laurent, 2018) and attentional GNN architectures (Brody et al., 2022; Vaswani et al., 2017) but did not see appreciable performance gain from using them. We introduced techniques borrowed from Transformer architectures such as pre-layer normalization (pre-LN) and residual connections (Xiong et al., 2020). Both mechanisms show an appreciable impact on performance. ReLU activations are applied after each convolutional layer and prior to skip connection combining.

The model is multi-headed, sharing a common feature extraction body. The value head is implemented as an MLP operating on globally pooled node features, while the action head is a shared MLP that processes the node features in the current action set independently.

*Remark 4.1.* We observed that increasing network depth generally degraded performance, even when attentional mechanisms were present. This phenomenon suggests unresolved information propagation bottlenecks within GNN architectures, representing a promising topic for future investigation.

*Remark 4.2.* A key practical challenge in extending GNN-based designs to other Polar code variants lies in the absence of clearly established reliability relations among their synthetic channels. Learning such relations directly from decoder behavior constitutes an important avenue for future research.

#### 4.6. Model Training

Training is conducted in a heterogeneous multi-node Kubernetes cluster. Each training instance uses a single Nvidia A100-40GB GPU node for GNN training and rollout orchestration. The reward generation for each parallelized environment is handled by a 8-core CPU worker node running a multi-threaded C++ based genie-aided (GA) SCL8 Polar decoder simulator. The GA decoder removes dependency on a particular CRC polynomial, which is critical because the standard employs different CRC polynomials for uplink and downlink. SCL8 is a successive cancellation decoder implementation with a list size of 8.

The BLER simulation employs a maximum of 500,000 transmitted blocks and terminates early after 500 block errors to ensure high precision evaluation. Training continues until completion of the entire reliability sequence, independent of the total number of timesteps.

The Adam optimizer is used (Kingma & Ba, 2017) with a fixed learning rate of  $2.5 \times 10^{-4}$ . PPO hyper parameters are as follows: 32 rollout steps per update, batch size of 256, 10 epochs, clip range 0.1, discount factor  $\gamma = 1.0$ , and a lookahead window of 16. Sixteen parallel environments are executed concurrently. Specific to the GNN architecture, three convolutional layers are used, the initial embedding size and hidden features size are 64 for all convolutional layers. Both the value head and per node action head use an MLP with 2 hidden layers with 128 and 32 units respectively.

To maximize hardware utilization, the environment and rollout routines were modified to support asynchronous reward generation. Because reward signals are available only at episode termination and episode lengths are uniformly random, the default synchronous per step reward generation leads to low utilization, as only a subset of processes complete episodes at any given step. Instead, we implement a “lazy” rollout strategy that queues reward-generation requests during rollouts and processes them collectively at the end of each horizon, significantly increasing the throughput by maximizing utilization of the available CPU resources.

Training proceeds iteratively: initially 1,000 episodes are used to learn the first 16 bit channels selections. Learning continues until the greedy policy consistently converges to the 16 selections (irrespective of order) across three consecutive evaluations. Thereafter the model learns subsequent

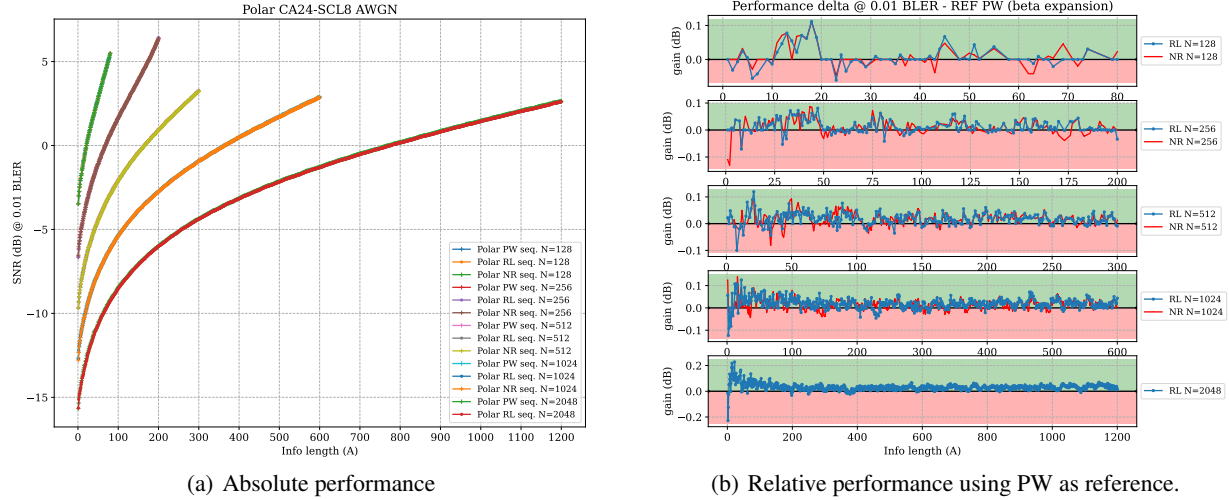


Figure 4. Polar code performance under CRC-aided successive cancellation list decoding over an AWGN channel for the beta expansion (PW), NR and RL-learned reliability sequences.

indices in pairs, requiring convergence to the same ordered selection for three consecutive evaluations before proceeding. This iterative procedure repeats until the full sequence is generated.

The majority of the overall training time is concentrated in the final progression (from N1024 to N2048), which required more than 30 days on the described cluster.

#### 4.7. Pretraining

Although pretraining is not critical to the quality of the learned sequence, we nonetheless used a pretrained GNN for the final learning run to reduce the time required for settling to a stable solution. We used the GNN trained using our initial training method. This method is detailed in Appendix B.

### 5. Simulation Results

All sequences considered are evaluated using the NR CRC24C polynomial (3GPP, 2020), with BPSK modulation over an AWGN channel. CRC-aided SCL decoding with a list size of 8 is used throughout all experiments. The code blocks are constructed directly from the Polar transform without rate matching. The BLER vs SNR performance is evaluated across the waterfall region in 0.5dB increments. At each SNR point a maximum of 500,000 blocks and a maximum limit of 500 block errors is simulated. The required SNR to achieve 1% BLER is extracted for each configuration and compared against the baseline beta expansion (PW) and the NR reliability sequence. Evaluations cover all

supported code rates up to approximately  $CR = 0.6$ .

In Figure 4(b), results are presented relative to the beta-expansion (PW) baseline. The relative performance of the NR sequence is also plotted for comparison. The RL-based method matches the performance of the NR sequence and, in particular, delivers consistent gains over the beta-expansion sequence at  $N = 2048$ . Both the learned sequence and NR sequence outperform the beta-expansion baseline with high probability. The learned sequence is included in Appendix A.

### 6. Conclusion

We present the first demonstration of a reinforcement-learning based universal sequence design at industrial scale, thereby making the approach practical for Polar code design in future communication system standardization efforts. We highlighted the critical use of the universal partial order – a law governing the relative reliability of the polarization induced synthetic channels – in constraining the search space and improving training efficiency. We also emphasized the advantage of joint multi-configuration optimization, which enables knowledge transfer across multiple code configurations and enhances learning efficiency.

Future work will explore extending this methodology to other Polar code variants by directly learning their intrinsic reliability structures and decoding specific properties, further advancing the data-driven design of channel coding techniques.

## References

3GPP. 5G NR Multiplexing and channel coding. Technical Specification (TS) 38.212 V16.2.0, 3rd Generation Partnership Project (3GPP), 2020. Release 16.

Arikan, E. Channel polarization: A method for constructing capacity-achieving codes for symmetric binary-input memoryless channels. *IEEE Transactions on information Theory*, 55(7):3051–3073, 2009.

Bioglio, V., Condo, C., and Land, I. Design of polar codes in 5G new radio. *IEEE Communications Surveys & Tutorials*, 23(1):29–40, 2020.

Bresson, X. and Laurent, T. Residual gated graph convnets, 2018. URL <https://arxiv.org/abs/1711.07553>.

Brody, S., Alon, U., and Yahav, E. How attentive are graph attention networks?, 2022. URL <https://arxiv.org/abs/2105.14491>.

Finn, C., Abbeel, P., and Levine, S. Model-agnostic meta-learning for fast adaptation of deep networks. In *International conference on machine learning*, pp. 1126–1135. PMLR, 2017.

Hamilton, W., Ying, Z., and Leskovec, J. Inductive representation learning on large graphs. *Advances in neural information processing systems*, 30, 2017.

He, G., Belfiore, J.-C., Land, I., Yang, G., Liu, X., Chen, Y., Li, R., Wang, J., Ge, Y., Zhang, R., et al. Beta-expansion: A theoretical framework for fast and recursive construction of polar codes. In *GLOBECOM 2017-2017 IEEE Global Communications Conference*, pp. 1–6. IEEE, 2017.

Hessel, M., Modayil, J., Van Hasselt, H., Schaul, T., Ostrovski, G., Dabney, W., Horgan, D., Piot, B., Azar, M., and Silver, D. Rainbow: Combining improvements in deep reinforcement learning. In *Proceedings of the AAAI conference on artificial intelligence*, volume 32, 2018.

Karniadakis, G. E., Kevrekidis, I. G., Lu, L., Perdikaris, P., Wang, S., and Yang, L. Physics-informed machine learning. *Nature Reviews Physics*, 3(6):422–440, 2021.

Kingma, D. P. and Ba, J. Adam: A method for stochastic optimization, 2017. URL <https://arxiv.org/abs/1412.6980>.

Liao, Y., Hashemi, S. A., Cioffi, J. M., and Goldsmith, A. Construction of polar codes with reinforcement learning. *IEEE Transactions on Communications*, 70(1):185–198, 2021.

Liao, Y., Hashemi, S. A., Yang, H., and Cioffi, J. M. Scalable polar code construction for successive cancellation list decoding: A graph neural network-based approach. *IEEE Transactions on Communications*, 71(11):6231–6245, 2023.

Liu, Z., Yao, L., Li, Y., Zhang, H., Wang, J., Yan, G., and Ma, Z. Partial orders in rate-matched polar codes. *arXiv preprint arXiv:2410.21661*, 2024.

Mishra, S. K., Katyal, D., and Ganapathi, S. A. A modified Q-learning algorithm for rate-profiling of polarization adjusted convolutional (PAC) codes. In *2022 IEEE Wireless Communications and Networking Conference (WCNC)*, pp. 2363–2368. IEEE, 2022.

Mnih, V., Kavukcuoglu, K., Silver, D., Rusu, A. A., Veness, J., Bellemare, M. G., Graves, A., Riedmiller, M., Fidjeland, A. K., Ostrovski, G., et al. Human-level control through deep reinforcement learning. *nature*, 518(7540):529–533, 2015.

Mondelli, M., Hassani, S. H., and Urbanke, R. L. Construction of polar codes with sublinear complexity. *IEEE Transactions on Information Theory*, 65(5):2782–2791, 2018.

Muller, D. E. Application of boolean algebra to switching circuit design and to error detection. *Transactions of the IRE professional group on electronic computers*, 4(3):6–12, 1954.

Okabe, R., Cheng, M., Chottrattanapituk, A., Mandal, M., Mak, K., Córdova Carrizales, D., Hung, N. T., Fu, X., Han, B., Wang, Y., et al. Structural constraint integration in a generative model for the discovery of quantum materials. *Nature Materials*, pp. 1–8, 2025.

Raffin, A., Hill, A., Gleave, A., Kanervisto, A., Ernestus, M., and Dormann, N. Stable-baselines3: Reliable reinforcement learning implementations. *Journal of Machine Learning Research*, 22(268):1–8, 2021. URL <http://jmlr.org/papers/v22/20-1364.html>.

Reed, I. A class of multiple-error-correcting codes and the decoding scheme. *Transactions of the IRE Professional Group on Information Theory*, 4(4):38–49, 1954. doi: 10.1109/TIT.1954.1057465.

Schulman, J., Wolski, F., Dhariwal, P., Radford, A., and Klimov, O. Proximal policy optimization algorithms, 2017. URL <https://arxiv.org/abs/1707.06347>.

Schürch, C. A partial order for the synthesized channels of a polar code. In *2016 IEEE International Symposium on Information Theory (ISIT)*, pp. 220–224. IEEE, 2016.

Vaswani, A., Shazeer, N., Parmar, N., Uszkoreit, J., Jones, L., Gomez, A. N., Kaiser, L., and Polosukhin, I. Attention is all you need. *Advances in neural information processing systems*, 30, 2017.

Xiong, R., Yang, Y., He, D., Zheng, K., Zheng, S., Xing, C., Zhang, H., Lan, Y., Wang, L., and Liu, T. On layer normalization in the transformer architecture. In *International conference on machine learning*, pp. 10524–10533. PMLR, 2020.

Yao, L., Liu, Z., Li, Y., Zhang, H., Wang, J., Yan, G., and Ma, Z.-M. New partial orders of polar codes for BMSC. In *2024 IEEE International Symposium on Information Theory (ISIT)*, pp. 2192–2197. IEEE, 2024.

## A. Learned sequence

The following are side by side comparison of the RL-learned sequence, the beta expansion (PW) sequence and the NR sequence.

RL	0	1	2	4	8	16	3	32	5	6	9	64	10	17	12	18	128	33	20	34	256	24	7	36	65	11	66	512	40	19	13	48
PW	0	1	2	4	8	16	3	32	5	6	9	64	10	17	12	18	128	33	20	34	7	24	36	65	11	256	66	40	13	19	68	14
RL	68	14	129	21	130	72	1024	35	257	22	132	25	80	37	136	26	41	38	67	258	513	96	514	28	42	69	144	49	131	73	70	44
PW	129	48	21	72	130	35	22	25	512	132	37	80	26	38	257	67	136	41	28	258	96	69	42	15	144	49	260	70	44	73	131	50
RL	160	260	516	264	1025	1026	272	288	15	50	133	74	23	81	52	137	134	76	27	82	56	192	520	39	259	97	138	528	145	29	84	43
PW	23	1024	264	74	160	513	133	52	81	27	76	514	134	39	272	82	137	56	29	516	259	192	97	138	84	43	30	145	288	98	261	71
RL	261	265	30	98	320	1028	1032	146	140	88	71	45	100	161	515	544	517	51	148	75	46	104	262	266	1040	273	77	53	152	162	193	83
PW	520	140	45	88	146	51	262	100	1025	46	265	75	161	528	148	53	320	1026	266	104	77	162	515	135	54	273	83	152	57	1028	268	78
RL	78	54	112	268	384	1056	521	576	640	289	57	164	274	1027	135	85	139	518	529	58	168	276	86	99	89	60	141	194	522	545	290	1029
PW	544	164	517	274	193	112	139	85	58	31	1032	518	384	289	194	99	276	168	86	521	141	60	89	147	290	576	263	196	101	522	142	1040
RL	1088	147	196	280	321	90	101	176	149	142	31	105	200	524	263	292	1033	1030	322	1152	92	102	267	153	163	530	546	150	47	106	165	208
PW	47	280	90	176	529	149	292	102	321	1027	524	267	200	105	92	163	530	150	55	322	1056	153	296	1029	106	269	79	640	545	165	532	275
RL	324	296	269	385	768	1041	1034	1042	577	532	536	275	79	108	55	154	87	113	304	195	548	166	270	114	328	277	169	156	386	197	177	59
PW	208	113	154	324	59	1030	270	108	546	1033	166	519	385	304	195	114	277	169	87	536	156	61	1088	328	1034	548	386	291	224	577	278	197
RL	170	224	552	519	578	1280	1057	1036	291	523	91	116	336	1058	1044	278	281	388	641	1089	1048	580	61	201	103	178	293	107	120	198	143	172
PW	170	116	523	143	1041	62	281	91	177	1036	768	578	388	293	198	103	552	336	172	1042	525	282	201	120	93	178	531	151	294	580	323	1152
RL	392	525	584	531	560	282	323	592	642	297	294	352	1060	1064	93	62	284	151	202	180	209	400	533	526	644	769	1536	1031	1035	1153	1090	547
PW	1057	526	392	297	202	1044	107	284	94	641	560	180	533	209	352	1058	155	325	298	1031	584	271	204	109	642	547	1048	167	534	400	305	210
RL	534	325	155	204	305	298	94	115	184	109	210	770	549	326	300	329	1154	1092	167	225	271	387	306	110	171	117	157	212	330	1043	416	537
PW	115	184	326	537	1060	157	300	1089	110	329	1035	644	549	387	306	225	592	279	212	171	117	538	158	1280	63	1090	330	1064	550	416	1037	769
RL	648	1072	1037	550	538	608	553	337	308	158	173	216	118	226	579	656	1045	389	332	279	121	179	228	393	199	390	338	312	448	561	672	581
PW	226	579	389	308	199	648	118	553	337	173	1043	540	283	216	121	1092	332	179	1038	770	608	390	295	228	581	554	338	1153	174	1072	527	393
RL	353	772	1281	1038	1046	1059	1282	1096	1104	1156	554	540	283	174	203	181	122	63	205	232	562	585	394	295	340	1049	1061	1284	401	643	556	582
PW	312	203	1045	122	285	95	656	561	181	1096	772	582	448	353	1154	1059	556	394	340	299	232	1046	585	286	205	124	643	562	1049	182	535	401
RL	354	285	299	124	182	211	240	776	527	593	564	645	586	535	784	1160	1091	1537	1120	1062	344	402	1050	1065	1168	704	396	185	307	286	95	206
PW	211	354	1536	185	327	1156	776	1061	586	396	301	206	1104	111	672	344	1050	645	564	402	307	240	593	213	186	356	539	1062	159	1281	302	1091
RL	213	186	327	356	417	646	649	588	301	594	360	302	331	111	309	404	539	568	609	771	800	1052	1093	1184	1538	1066	1155	1094	1288	551	657	217
PW	588	331	1160	1065	646	551	417	1052	784	227	594	404	309	214	649	119	568	188	1282	541	1120	217	360	1093	1066	333	418	1039	771	704	609	391
RL	188	214	227	368	408	313	333	339	418	650	1073	1097	1074	541	596	310	159	119	229	391	334	420	218	175	220	233	449	1296	600	555	610	652
PW	310	229	650	596	555	339	1168	175	1073	542	408	313	218	1284	123	1094	334	657	1068	800	610	420	1097	773	230	583	449	368	1155	652	1074	557
RL	773	1105	658	673	583	542	832	1157	1039	1047	1216	1068	777	612	557	314	341	1540	1076	1098	123	563	316	230	355	424	395	345	125	183	234	397
PW	395	341	314	233	1047	600	287	220	125	658	563	1288	183	1098	774	612	450	355	1194	1537	558	424	342	1157	777	234	1076	587	397	316	207	1105

Figure 5. Comparison of RL-learned sequence vs beta expansion at  $N = 2048$ , first part.

RL	432	450	587	660	1106	1158	1080	1312	241	674	1161	616	774	342	403	785	778	565	1051	1544	1063	357	398	207	187	236	346	215	242	287	452	558
PW	126	673	345	1051	660	565	403	241	1100	832	1538	452	187	357	1158	778	1063	616	398	1296	303	236	1106	589	674	346	1161	1080	647	566	432	1053
RL	1162	1121	1283	1122	664	1100	705	624	786	896	358	361	405	348	126	456	569	595	589	566	676	1552	1108	1169	1170	1285	780	647	1344	706	801	419
PW	785	242	595	405	215	664	358	569	1540	189	1283	1216	780	1121	590	456	361	1162	1108	1067	676	348	419	1054	786	705	624	406	311	244	651	597
RL	1053	680	590	189	219	244	303	406	1185	369	409	248	362	311	464	1164	1286	1067	1095	1112	1075	1124	1054	1539	570	651	597	611	802	788	421	601
PW	570	1169	190	1312	543	409	1122	219	1285	362	1095	1544	335	1164	896	1069	801	706	611	421	1112	788	231	680	598	464	369	1170	653	1075	572	410
RL	708	1289	1568	1069	1297	653	572	688	792	231	335	364	190	598	1128	1290	659	425	221	422	370	451	372	410	613	235	343	315	317	480	712	833
PW	315	248	1286	601	1124	221	364	659	1070	802	1289	422	1099	775	708	613	451	370	1185	654	1552	559	425	343	1172	792	235	1077	602	412	317	222
RL	1186	1172	543	804	1408	1077	1099	1313	1070	412	654	661	602	453	775	1292	1298	1136	1541	1188	1078	1314	1107	614	617	376	222	834	1600	1542	604	237
PW	1344	127	688	1290	661	1128	804	614	480	1101	833	1186	1539	453	426	372	1159	779	712	1078	617	399	1297	318	237	1107	604	675	347	1176	1081	662
RL	454	433	426	559	675	808	1081	1101	1217	1176	1159	1123	1082	1218	720	665	662	779	618	677	625	359	1192	318	347	243	399	127	238	434	457	428
PW	567	433	1292	243	1102	834	1568	454	665	359	1188	808	1541	618	428	1298	1217	781	238	1136	591	457	376	1163	1109	1082	677	349	434	1055	787	720
RL	836	816	1102	897	567	1163	1545	1546	787	245	781	736	591	626	1109	1110	666	458	620	707	349	782	571	436	363	1287	1300	407	350	465	789	681
PW	625	407	245	666	836	571	1542	1408	191	1313	1218	782	1123	620	458	1300	363	1192	1110	1545	678	350	1165	897	1084	816	707	626	436	1113	789	246
RL	840	678	898	599	668	803	1345	1346	1316	1220	1125	1553	1554	1055	1548	1171	1664	1165	1166	1113	1114	1304	628	460	246	573	709	249	423	1084	371	1200
PW	681	599	465	1171	668	1314	573	411	1600	249	1287	1220	840	1125	1546	460	365	1166	898	1071	803	736	1304	423	1114	790	709	682	628	466	371	1200
RL	440	466	682	1224	689	411	365	848	250	413	366	191	373	468	481	805	793	900	790	1173	1320	1116	1556	1348	1126	1174	1129	1232	1177	1569	1187	1409
PW	655	1553	574	440	1173	793	250	1316	603	413	1126	223	1345	366	689	1548	1291	1224	900	1129	805	710	615	481	1116	848	1187	684	1554	468	427	373
RL	632	603	713	615	710	690	684	574	655	835	414	427	223	374	252	482	794	809	605	619	721	904	1291	1328	1189	1071	1293	1137	806	864	1570	1560
PW	1174	794	713	1079	632	414	319	252	1346	605	690	1177	1320	663	1130	806	1293	482	1103	835	1664	1569	455	904	374	1189	809	714	1556	619	429	1299
RL	1130	1079	1248	1572	714	663	692	1132	1193	429	455	319	435	377	472	484	837	817	796	912	1601	1178	1352	1299	1792	1219	1190	1103	1138	1410	1294	810
PW	1232	796	239	1137	606	472	377	1178	1348	1083	692	435	1294	721	1132	864	1570	484	667	837	1190	810	1543	1409	430	1328	1219	783	716	1138	621	459
RL	679	722	627	737	667	621	378	437	459	696	899	716	488	1543	1301	1602	1180	1083	1221	430	461	239	669	606	1412	1315	1140	818	841	838	1111	1201
PW	1301	378	1193	1111	1560	679	351	1180	912	1085	817	722	627	437	1352	247	696	838	1572	1410	669	1315	1248	812	1601	622	488	1302	1221	841	1194	1140
RL	629	928	812	738	622	724	1576	1360	1547	1194	1665	1085	1302	1305	820	849	380	351	467	1317	1604	1225	1202	1416	1222	1144	438	1196	441	469	247	630
PW	1547	461	380	1167	899	1086	818	737	1305	438	1115	791	724	683	629	467	1201	670	1792	575	441	1602	1412	251	1317	1222	842	1127	1576	462	1360	367
RL	415	462	367	496	740	728	901	783	1584	1167	791	711	683	1086	1376	1127	1318	1549	1204	691	670	902	842	1555	1306	1321	1115	850	685	633	960	844
PW	1196	928	1549	738	1306	1225	901	1144	820	711	630	496	1117	849	1202	685	1555	469	442	1175	795	728	1318	633	415	1604	253	1347	844	691	1550	1416
RL	905	442	1424	1226	1175	1308	1666	1550	1233	375	483	575	473	444	1117	1329	1608	1228	1347	470	251	807	865	715	795	686	824	1557	1349	1668	1131	1133
PW	1321	1226	902	1131	807	740	1308	483	1118	850	1665	686	1584	470	905	375	1204	824	715	1557	634	444	1233	797	254	1376	607	473	1179	1349	1322	693
RL	1249	1571	693	744	1616	1573	1353	634	852	636	797	906	811	717	485	379	431	489	474	253	1322	1191	1793	1118	1234	1208	1561	1139	1440	1324	1179	1350
PW	1608	1293	1228	960	1133	865	1666	1571	485	906	852	1191	811	744	1558	1424	431	1329	1234	798	717	1139	636	474	379	1208	1350	1561	694	1181	913	1324

 Figure 6. Comparison of RL-learned sequence vs beta expansion  $N = 2048$ , second part.

RL	913	723	752	697	607	866	1295	1558	1411	1330	1632	1672	1134	856	694	813	908	1181	1236	1195	1354	819	486	381	476	463	439	490	492	497	254	718
PW	723	1134	866	1353	486	697	839	1668	1573	1411	908	1330	1249	813	718	1616	623	489	1303	1236	856	1195	1141	1562	476	381	1182	914	1087	819	752	439
RL	914	868	1562	1250	1141	698	725	623	839	739	929	1603	1413	1361	798	1574	1240	1322	1794	1182	1252	1472	1223	1303	1414	1356	1680	1577	1142	1197	1362	1564
PW	1354	725	698	866	1574	1440	671	1793	1250	814	1603	1413	490	1332	1223	843	1672	1142	1577	463	1361	382	1197	929	1564	739	1307	1240	916	1145	821	726
RL	1605	814	872	930	726	1145	700	843	631	729	821	671	741	916	1417	1256	1336	1087	1796	1203	1307	1146	1198	1377	1585	822	382	443	445	471	498	880
PW	631	497	1356	1203	700	1794	443	1632	1414	729	1319	1252	872	1605	1578	492	1362	845	1198	930	1551	1417	1336	1227	903	1146	822	741	1309	498	1119	851
RL	920	1578	1319	1227	1418	1696	1609	730	845	851	635	825	745	742	932	826	687	903	961	1378	1580	1323	1800	1205	1364	1425	1606	1667	1309	1551	1229	1586
PW	1680	687	1585	471	920	1205	825	730	1796	635	445	1606	1472	255	1377	846	1580	1418	1364	1323	1256	932	1609	742	1310	1229	961	1148	880	1667	1586	500
RL	1264	500	1209	936	1235	846	732	907	1148	1119	962	1368	1420	853	1610	1617	1310	1426	753	637	746	695	828	487	475	1206	1669	1808	477	446	478	504
PW	907	853	1206	826	745	1559	1425	446	1235	799	732	1378	637	475	1209	1351	1800	695	1610	1420	1325	1230	962	1135	867	1696	1368	487	936	854	1669	746
RL	944	909	867	1441	1325	1230	1673	1380	1351	964	854	748	915	857	1728	1384	1331	1588	1612	1559	1210	1237	1592	1251	1135	1633	754	869	638	719	491	493
PW	1588	1426	909	1331	1264	828	719	1617	638	504	1237	857	1210	1380	1563	477	1183	915	1326	753	1612	1355	964	699	869	1670	1575	1441	910	1808	1251	815
RL	255	1442	1618	1428	1824	1670	699	799	858	910	968	1212	1326	1563	1241	1355	1253	1432	1392	1238	1333	917	756	870	727	860	873	1575	1681	1473	1620	1183
PW	748	1618	1428	491	1333	1238	858	1673	1143	1592	478	383	1212	944	1565	754	1241	917	1384	727	870	1357	1442	701	1795	1728	1633	1415	968	1334	1253	873
RL	1795	1143	1337	701	815	931	1444	921	976	1565	1363	1357	918	760	499	1674	1634	1242	1324	1415	1257	1624	1797	1254	1579	1682	1676	1474	1199	1448	1419	1566
PW	1674	1620	1579	493	1363	860	1199	931	1566	1432	1337	1242	918	1147	823	756	499	1358	1681	702	1824	921	1634	1444	731	1797	1254	874	1607	1473	494	1392
RL	1244	1147	1697	881	383	1338	731	874	933	702	823	743	501	922	1358	1365	1587	1856	1636	494	1379	733	876	847	882	827	937	992	1801	1607	934	963
PW	847	1676	1581	1419	1365	1338	1257	933	1624	743	1311	1244	976	1149	881	1682	1587	501	922	1207	827	760	1798	447	1636	1474	733	1379	876	1582	1448	1366
RL	1265	1798	1581	1456	1684	1207	1258	1149	1427	747	505	1369	1366	1611	1698	1476	1311	1421	1809	1640	1340	829	884	855	924	502	1266	1802	1589	1381	1370	1231
PW	1801	1258	934	1611	1421	1340	1231	963	1150	882	1697	1369	502	937	855	1684	747	1589	1427	924	1265	829	734	1856	639	505	1476	1211	1381	1802	1640	1422
RL	1150	1582	1619	1211	1260	1480	1688	1422	945	734	639	938	965	888	755	447	1729	1648	1382	1613	1590	1385	1700	749	859	830	871	506	1268	1593	1804	1810
PW	1327	1260	992	1613	1698	1370	965	938	884	1671	1590	1456	911	1809	1266	830	749	1619	1429	506	1239	859	1688	1382	1593	479	1213	945	1804	755	1614	1480
RL	1671	1920	1429	1372	1239	1488	1327	1443	1213	1430	946	940	969	757	966	1433	1730	1272	750	911	861	875	508	1393	1621	1614	1594	1386	1335	1812	1825	948
PW	1385	966	871	1700	1372	1443	940	1810	1729	750	1648	1430	969	1335	1268	888	1675	1621	1594	508	861	1214	946	1567	1433	1243	919	1386	757	1359	1920	703
RL	761	919	479	1445	1704	1214	1243	977	1504	970	1434	1675	1635	1388	1255	1732	1622	1359	1625	1475	1394	1245	1826	1677	1567	1816	1683	862	1339	1857	1596	1712
PW	1825	1730	1635	1445	970	1812	1255	875	1704	1622	1488	495	1393	862	1677	1596	1434	1339	1272	948	1625	758	1245	977	1388	1683	1826	923	1446	761	1799	1732
RL	1637	703	952	883	758	923	877	762	978	1446	1449	993	935	972	1396	1436	925	885	495	1736	1259	1457	1828	1685	1477	1799	1367	1341	1626	1450	1246	1678
PW	1637	1475	972	1394	877	1678	1583	1449	1367	1816	1259	935	1626	1436	1341	1246	978	1151	883	1712	503	952	1685	762	1828	925	1638	1504	735	1857	878	1477
RL	1641	1267	1858	1699	1638	1744	1458	1261	939	735	980	878	764	503	1832	1400	1481	1478	1452	1583	994	1151	1628	1689	1803	1371	1342	1423	1383	1686	1921	1701
PW	1450	1396	1803	1736	1641	1423	1342	1261	993	1628	1699	1371	980	939	885	1686	1591	1457	926	1267	831	764	1858	507	1478	1689	1383	1832	1642	1452	1805	1262
RL	1642	926	886	889	831	941	947	984	1649	1860	1262	1482	1269	1591	1489	1805	1811	1373	1840	1615	1731	1644	1864	967	1760	1387	1650	751	996	890	942	507
PW	994	1613	1481	1400	967	886	1701	1373	1458	941	1811	1744	751	1649	1431	984	1269	889	1690	1860	1595	509	1215	947	1806	1644	1482	1387	996	1702	1374	1921

 Figure 7. Comparison of RL-learned sequence vs beta expansion  $N = 2048$ , third part.

RL	1431	1690	1273	1460	1270	1705	1702	1595	971	1374	1490	1806	1623	1922	1484	949	863	509	1733	1395	1505	1813	1389	1827	1215	950	1000	1435	1652	1447	1713	1464
PW	942	1840	1731	1650	1460	971	1813	1270	890	1705	1623	1489	510	863	1692	1597	1435	1273	949	1864	759	1484	1389	1922	1827	1760	1447	1000	1814	1733	1706	1652
RL	1692	973	892	953	759	1706	1597	1872	1274	1817	979	1492	1814	974	954	879	1008	1656	1924	1397	1506	1437	1829	1737	1627	1451	1390	1714	1734	763	1639	1276
PW	1490	973	1395	892	1679	1598	1464	1817	1274	950	1627	1437	1247	979	1390	1713	953	1924	763	1829	1734	1639	1505	974	1872	879	1708	1492	1451	1397	1818	1737
RL	1598	1247	1708	1888	1679	1833	1401	1818	1496	1928	1716	1629	1745	1453	1508	995	981	765	1830	1459	1859	1738	1398	1936	1438	1687	1820	1643	1630	1834	1479	1263
PW	1656	1438	1343	1276	1008	1629	1714	981	954	1687	1830	927	1506	765	1859	1479	1928	1398	1833	1738	1643	1453	1820	1263	995	1630	1496	1401	982	887	1716	1459
RL	1343	1861	1402	887	927	956	985	982	997	891	943	986	1001	998	893	510	1512	1740	1454	1483	1746	1720	1841	1645	1862	1646	1461	1691	1761	1651	1836	1703
PW	956	1745	766	1888	985	1508	1691	1861	1834	1454	1807	1740	1645	1483	1402	997	1703	1375	1936	943	1841	1746	1651	1461	986	1271	891	1720	1862	511	1693	1836
RL	1271	1404	1865	1952	1520	1748	1485	1693	1465	1842	1807	1923	951	766	1462	1375	1491	988	1707	1762	1694	1866	511	1925	1486	1275	1002	1844	1752	1653	1009	1654
PW	1646	1512	1865	998	1485	1404	1923	1842	1761	1462	1001	1815	1748	1707	1653	1491	988	893	1694	1599	1465	1275	951	1866	1486	1391	1952	1762	1925	1002	1844	1735
RL	1873	1466	1507	1815	1493	1764	1391	1735	1715	1709	1657	1277	975	1929	1868	1004	1010	1497	1984	1599	955	1889	1926	1819	1848	1768	1874	1509	1468	1439	894	1717
PW	1654	1520	975	1873	894	1709	1493	1466	1819	1752	1657	1439	1277	1009	1868	1715	955	1926	1831	1764	1507	1004	1874	1710	1494	1929	1399	1848	1739	1658	1468	1821
RL	1831	1658	1494	1399	1739	1937	1012	1710	957	1513	1278	1776	1721	1930	1498	983	1876	1747	1660	1835	1890	1821	1403	1741	1455	1631	767	1016	987	1510	1718	1822
PW	1278	1010	1631	1497	983	1717	957	1984	767	1889	1509	1930	1876	1835	1768	1455	1822	1741	1660	1498	1403	1012	1718	1937	958	1747	1890	987	1510	1721	1863	1932
RL	1880	1521	1722	958	1938	1843	1500	1863	1742	1892	1749	1405	1514	1463	1953	1932	999	1837	1763	1647	989	1753	1003	1867	1896	1845	1724	1940	1522	1516	1750	1467
PW	1837	1742	1647	1513	1880	999	1500	1405	1938	1843	1776	1463	1016	1749	1722	1892	989	1695	1838	1514	1867	1487	1406	1953	1763	1940	1003	1845	1750	1655	1521	990
RL	1838	1695	1944	1487	1754	1954	1985	990	1875	1655	1765	1849	1406	1869	1904	1005	1469	1769	1011	1846	1659	1524	1495	1927	1850	1877	1956	895	1499	1279	1528	1711
PW	895	1724	1467	1753	1896	1516	1869	1954	1927	1846	1765	1522	1005	1875	1711	1495	1944	1849	1754	1659	1469	1279	1011	1870	1956	1766	1985	1006	1904	1524	1931	1877
RL	1870	1931	1766	1770	1986	1891	1756	1661	1006	1823	1960	1719	1470	1777	1881	1013	1878	1511	1852	1662	1501	1933	1968	1017	1939	1723	1778	1772	1988	1893	1882	1743
PW	1850	1769	1470	1823	1756	1661	1499	1013	1719	959	1986	1891	1511	1960	1878	1770	1933	1852	1743	1662	1528	1881	1014	1501	1939	1777	1017	1988	1723	1893	1934	1839
RL	1515	1014	1018	1992	1934	1941	1894	1780	1517	1784	1751	1502	1897	1523	1725	1839	1955	959	1884	1726	1942	2000	1945	1525	1847	1898	1407	1905	1755	1957	1020	1946
PW	1772	1515	1882	1502	1407	1968	1778	1941	1018	1751	1894	991	1725	1992	1897	1517	1884	1955	1942	1847	1780	1523	1020	1726	1945	1755	1898	1518	1871	1957	1767	2000
RL	1518	1767	1757	1906	1871	1900	1851	1958	1529	1961	1771	2016	1987	991	1948	1962	1758	1879	1908	1853	1526	1471	1989	1969	1854	1530	1663	1912	1007	1773	1964	1779
PW	1007	1905	1525	1946	1851	1784	1471	1757	1900	1958	1867	1906	1526	1961	1879	1771	1948	1853	1758	1663	1529	1015	2016	1989	1962	1908	1935	1854	1773	1530	1883	1503
RL	1883	1935	1990	1774	1895	1532	1993	1790	1885	1503	1781	1015	1899	1943	1972	2001	1994	1727	1519	1886	1785	1782	1947	1907	1901	1976	2002	1996	1786	1019	1959	2049
PW	1669	1779	1019	1990	1895	1964	1774	1993	1912	1532	1885	1970	1943	1781	1021	1727	1994	1899	1519	1886	1972	1782	2001	1022	1947	1785	1996	1901	1959	2002	1907	1527
RL	2017	1909	1902	1759	2004	1963	1527	1788	1855	1913	1950	1808	1021	1991	1910	1965	1791	1531	1775	2020	1914	1995	1887	1973	1022	1966	1997	2024	1916	1533	2003	
PW	1976	1786	1949	1759	1902	2017	2004	1963	1909	1950	1855	1788	1531	2018	1991	1910	1965	1775	2008	1913	1533	1971	2020	1966	1995	1914	1534	1887	1973	1783	1023	2024
RL	1783	1977	1974	1903	1998	2005	2032	1787	1951	1978	2009	1534	2006	1789	2019	1980	1911	2021	1910	1967	2022	1790	2012	2025	1915	1917	1999	2026	1023	2028	1975	1918
PW	1997	1916	1974	2003	1977	1787	1998	1903	2032	2005	1978	1951	1789	2019	2006	1911	1980	1790	2009	2021	1967	2010	1915	1535	2022	2025	1917	1975	2026	1999	1918	
RL	2033	2007	2034	2023	2036	1535	1979	1981	1982	1791	2011	2013	2027	2029	2040	2014	2030	1919	2035	2037	2038	1983	2041	2015	2031	2042	2044	2039	2043	2045	2046	2047
PW	2033	1979	2028	2034	2007	1981	1791	2036	1982	2011	2023	2040	2013	2027	2014	1919	2029	2035	2030	2037	1983	2038	2041	2042	2015	2044	2031	2039	2043	2045	2046	2047

 Figure 8. Comparison of RL-learned sequence vs beta expansion  $N = 2048$ , fourth part.

RL	0	1	2	4	8	16	3	32	5	6	9	64	10	17	12	18	128	33	20	34	256	24	7	36	65	11	66	512	40	19	13	48	
NR	0	1	2	4	8	16	32	3	5	64	9	6	17	10	18	128	12	33	65	20	256	34	24	36	7	129	66	512	11	40	68	130	
PW	0	1	2	4	8	16	3	32	5	6	9	64	10	17	12	18	128	33	20	34	7	24	36	65	11	256	66	40	13	19	68	14	
RL	68	14	129	21	130	72	35	257	22	132	25	80	37	136	26	41	38	67	258	513	96	514	28	42	69	144	49	131	73	70	44	160	
NR	19	13	48	14	72	257	21	132	35	258	26	513	80	37	25	22	136	260	264	38	514	96	67	41	144	28	69	42	516	49	74	272	
PW	129	48	21	72	130	35	22	25	512	132	37	80	26	38	257	67	136	41	28	258	96	69	42	15	144	49	260	70	44	73	131	50	
RL	260	516	264	272	288	15	50	133	74	23	81	52	137	134	76	27	82	56	192	520	39	259	97	138	528	145	29	84	43	261	265	30	
NR	160	520	288	528	192	544	70	44	131	81	50	73	15	320	133	52	23	134	384	76	137	82	56	27	97	39	259	84	138	145	261	29	
PW	23	264	74	160	513	133	52	81	27	76	514	134	39	272	82	137	56	29	516	259	192	97	138	84	43	30	145	288	98	261	71	520	
RL	98	320	146	140	88	71	45	100	161	515	544	517	51	148	75	46	104	262	266	273	77	53	152	162	193	83	78	54	112	266	384	521	
NR	43	98	515	88	140	30	146	71	262	265	161	576	45	100	640	51	148	46	75	266	273	517	104	162	53	193	152	77	164	768	268	274	
PW	140	45	88	146	51	262	100	46	265	75	161	528	148	53	320	266	104	77	162	515	135	54	273	83	152	57	268	78	544	164	517	274	
RL	576	640	289	57	164	274	135	85	139	518	529	58	168	276	86	99	89	60	141	194	522	545	290	147	196	280	321	90	101	176	149	142	
NR	518	54	83	57	521	112	135	78	289	194	85	276	522	58	168	139	99	86	60	280	89	290	529	524	196	141	101	147	176	142	530	321	
PW	193	112	139	85	58	31	518	384	289	194	99	276	168	86	521	141	60	89	147	290	576	263	196	101	522	142	47	280	90	176	529	149	
RL	31	105	200	524	263	292	322	92	102	267	153	163	530	546	150	47	106	165	208	324	296	269	385	768	577	532	536	275	79	108	55	154	
NR	31	200	90	545	292	322	532	263	149	102	105	304	296	163	92	47	267	385	546	324	208	396	150	153	165	106	55	328	536	577	549	113	
PW	292	102	321	524	267	200	105	92	163	530	150	55	322	153	296	106	269	79	640	545	165	165	327	275	208	113	154	324	59	270	108	546	166
RL	87	113	304	195	548	166	270	114	328	277	169	156	386	197	177	59	170	224	552	519	578	291	523	91	116	336	278	281	388	641	580	61	
NR	154	79	269	108	578	224	166	519	552	195	270	641	523	275	580	291	59	169	560	114	277	156	87	197	116	170	61	531	525	642	281	278	
PW	519	385	304	195	114	277	169	87	536	156	61	328	548	386	291	224	577	278	197	170	116	523	143	62	281	91	177	768	578	388	293	196	
RL	201	103	178	293	107	120	198	143	172	392	525	584	531	560	282	323	592	642	297	294	352	93	62	284	151	202	180	209	400	533	526	644	
NR	526	177	293	388	91	584	769	198	172	120	201	336	62	282	143	103	178	294	93	644	202	592	323	392	297	770	107	180	151	209	284	648	
PW	103	552	336	172	525	282	201	120	93	178	531	151	294	580	323	526	392	297	202	107	284	94	641	560	180	533	209	352	155	325	298	584	
RL	769	547	534	325	155	204	305	298	94	115	184	109	210	770	549	326	300	329	167	225	271	387	306	110	171	117	157	212	330	416	537	648	
NR	94	204	298	400	608	352	325	533	155	210	305	547	300	109	184	534	537	115	167	225	326	306	772	157	656	329	110	117	212	171	776	330	
PW	271	204	109	642	547	167	534	400	305	210	115	184	326	537	157	300	110	329	644	549	387	306	225	592	279	212	171	117	538	158	63	330	
RL	550	538	608	553	337	308	158	173	216	118	226	579	656	389	332	279	121	179	228	393	199	390	338	312	448	561	672	581	353	772	554	540	
NR	226	549	538	387	308	216	416	271	279	158	337	550	672	118	332	579	540	389	173	121	553	199	784	179	228	338	312	704	390	174	554	581	
PW	550	416	769	226	579	389	308	199	648	118	553	337	173	540	283	216	121	332	179	770	608	390	295	228	581	554	338	174	527	393	312		
RL	283	174	203	181	122	63	205	232	562	585	394	295	340	401	643	556	582	354	285	299	124	182	211	240	776	527	593	564	645	586	535	784	
NR	393	283	122	448	353	561	203	63	340	394	527	582	556	181	295	285	232	124	205	182	643	562	286	585	299	354	211	401	185	396	344	586	
PW	122	285	95	656	561	181	772	582	448	353	556	394	340	299	232	585	286	205	124	643	562	182	535	401	211	354	185	327	776	586	396	301	
RL	344	402	704	396	185	307	286	95	206	213	186	327	356	417	646	649	588	301	594	360	302	331	111	309	404	539	568	609	771	800	55	657	
NR	645	593	535	240	206	95	327	564	800	402	356	307	301	417	213	568	832	588	186	646	404	227	896	594	418	302	649	771	360	539	11	331	
PW	206	111	672	344	645	564	402	307	240	593	213	186	356	539	159	302	588	331	646	551	417	784	227	594	404	309	214	649	119	568	188	541	
RL	217	188	214	227	368	408	313	333	339	418	650	541	596	310	159	119	229	391	334	420	218	175	220	233	449	600	555	610	652	773	658	673	
NR	214	309	188	449	217	408	609	596	551	650	229	159	420	310	541	773	610	657	333	119	600	339	218	368	652	230	391	313	450	542	334	233	
PW	217	360	333	418	771	704	609	391	310	229	650	596	555	339	175	542	408	313	218	123	334	657	800	610	420	773	230	583	449	368	652	557	
RL	583	542	832	777	612	557	314	341	123	563	316	230	355	424	395	345	125	183	234	397	432	450	587	660	241	674	616	774	342	403	778		
NR	555	774	175	123	658	612	341	777	220	314	424	395	673	583	355	287	183	234	125	557	660	616	342	316	241	778	563	345	452	397	403	207	
PW	395	341	314	233	600	287	220	125	658	563	183	774	612	450	355	558	424	342	777	234	587	397	316	207	126	673	345	660	565	403	241	832	
RL	565	357	398	207	187	236	346	21																									

RL	659	425	221	422	370	451	372	410	613	235	343	315	317	480	712	833	543	804	412	654	661	602	453	775	614	617	376	222	834	604	237	454	
NR	364	654	659	335	480	315	221	370	613	422	425	451	614	543	235	412	343	372	775	317	222	426	453	237	559	833	804	712	834	661	808	779	
PW	659	802	422	775	708	613	451	370	654	559	425	343	792	235	602	412	317	222	127	688	661	804	614	480	833	453	426	372	779	712	617	399	
RL	433	426	559	675	808	720	665	662	779	618	677	625	359	318	347	243	399	127	238	434	457	428	836	816	897	567	787	245	781	736	591	626	
NR	617	604	433	720	816	836	347	897	243	662	454	318	675	618	898	781	376	428	665	736	567	840	625	238	359	457	399	787	591	678	434	677	
PW	318	237	604	675	347	662	567	433	243	834	454	665	359	808	618	428	781	238	591	457	376	677	349	434	787	720	625	407	245	666	836	571	
RL	666	458	620	707	349	782	571	436	363	407	350	465	789	681	840	678	898	599	668	803	628	460	246	573	709	249	423	371	440	466	682	689	
NR	349	245	458	666	620	363	127	191	782	407	436	626	571	465	681	246	707	350	599	668	790	460	249	682	573	411	803	789	709	365	440	628	
PW	191	782	620	458	363	678	350	897	816	707	626	436	789	246	681	599	465	668	573	411	249	840	460	365	898	803	736	423	790	709	682	628	
RL	411	365	848	250	413	366	191	373	468	481	805	793	900	790	632	603	713	615	710	690	684	574	655	835	414	427	223	374	252	482	794	809	
NR	689	374	423	466	793	250	371	481	574	413	603	366	468	655	900	805	615	684	710	429	794	252	373	605	848	690	713	632	482	806	427	904	
PW	466	371	655	574	440	793	250	603	413	223	366	689	900	805	710	615	481	848	684	468	427	373	794	713	632	414	319	252	605	690	663	806	
RL	605	619	721	904	806	864	714	663	692	429	455	319	435	377	472	484	837	817	796	912	810	679	722	627	737	667	621	378	437	459	696	899	
NR	414	223	663	692	835	619	472	455	796	809	714	721	837	716	864	810	606	912	722	696	377	435	817	319	621	812	484	430	838	667	488	239	
PW	482	835	455	904	374	809	714	619	429	796	239	606	472	377	692	435	721	864	484	667	837	810	430	783	716	621	459	378	679	351	912	817	
RL	716	488	430	461	239	669	606	818	841	838	629	928	812	738	622	724	820	849	380	351	467	438	441	469	247	630	415	462	367	496	740	728	
NR	378	459	622	627	437	380	818	461	496	669	679	724	841	629	351	467	438	737	251	462	442	441	469	247	683	842	738	899	670	783	849	820	
PW	722	627	437	247	696	838	669	812	622	488	841	461	380	899	818	737	438	791	724	683	629	467	670	575	441	251	842	462	367	928	738	901	
RL	901	783	791	711	683	691	670	902	842	850	685	633	960	844	905	442	375	483	575	473	444	470	251	807	865	715	795	686	824	693	744	634	
NR	728	928	791	367	901	630	685	844	633	711	253	691	824	902	686	740	850	375	444	470	483	415	485	905	795	473	634	744	852	960	865	693	
PW	820	711	630	496	849	685	469	442	795	728	633	415	253	844	691	902	807	740	483	850	686	470	905	375	824	715	634	444	797	254	607	473	
RL	852	636	797	906	811	717	485	379	431	489	474	253	913	723	752	697	607	866	856	694	813	908	819	486	381	476	463	439	490	492	497	254	
NR	797	906	715	807	474	636	694	254	714	717	575	913	798	811	379	697	431	607	489	866	723	486	908	718	813	476	856	839	725	698	914	752	868
PW	693	960	865	485	906	852	811	744	431	798	717	636	474	379	694	913	723	866	486	697	839	908	813	718	623	489	856	476	381	914	819	752	
RL	718	914	868	698	725	623	839	739	929	798	814	872	930	726	700	843	631	729	821	671	741	916	822	382	443	445	471	498	880	920	730	845	
NR	819	814	439	929	490	623	671	739	916	463	843	381	497	930	821	726	961	872	492	631	729	700	443	741	845	920	382	822	851	730	498	880	
PW	439	725	698	868	671	814	490	843	463	382	929	739	916	821	726	631	497	700	443	729	872	492	492	845	930	903	822	741	498	851	687	471	920
RL	851	635	825	745	742	932	826	687	903	961	500	936	846	732	907	962	853	753	637	746	695	828	487	475	477	446	478	504	944	909	867	964	
NR	742	445	471	635	932	687	903	825	500	846	745	826	732	446	962	936	475	853	867	637	907	487	695	746	828	753	854	857	504	799	255	964	
PW	825	730	635	445	255	846	932	742	961	880	500	907	853	826	745	446	799	732	637	475	695	962	867	487	936	854	746	909	828	719	638	504	
RL	854	748	915	857	754	869	638	719	491	493	255	699	799	858	910	968	917	756	870	727	860	873	701	815	931	921	976	918	760	499	881	383	
NR	909	719	477	915	638	748	944	869	491	699	754	858	478	968	383	910	815	976	870	917	727	493	873	701	931	756	860	499	731	823	922	874	
PW	857	477	915	753	964	699	869	910	815	748	491	858	478	383	944	754	917	727	870	701	968	873	493	860	931	918	823	756	499	702	921	731	
RL	731	874	933	702	823	743	501	922	494	733	876	847	882	827	937	992	934	963	747	505	829	884	855	924	502	945	734	639	938	965	888	755	
NR	918	502	933	743	760	881	494	702	921	501	876	847	992	447	733	827	934	882	937	963	747	505	855	924	734	829	965	938	884	506	749	945	
PW	874	494	847	933	743	976	881	501	922	827	760	447	733	876	934	963	882	502	937	855	747	924	829	734	639	505	992	965	938	884	911	830	
RL	447	749	859	830	871	506	946	940	969	757	966	750	911	861	875	508	948	761	919	479	977	970	862	703	952	883	758	923	877	762	978	993	
NR	966	755	859	940	830	911	871	639	888	479	946	750	969	508	861	757	970	919	875	862	758	948	977	923	972	761	877	952	495	703	935	978	
PW	749	506	859	479	945	755	966	871	940	750	969	888	508	861	946	919	757	703	970	875	495	862	948	738	977	923	761	972	877	935	978	883	
RL	935	972	925	885	495	939	735	980	878	764	503	994	926	886	889	831	941	947	984	967	855	924	751	942	996	971	890	509	949	973	1000	892	950
NR	883	762	503	925	878	735	993	885	939	994	980	926	764	941	967	886	831	947	507	889	984	751	942	99									

## B. GNN Pretraining

In this section, we describe the initial sequence learning method which was used to pretrain the model.

### B.1. Whole sequence learning with range expansion

For any sequence length  $N \leq 512$ , all configurations are optimized jointly: the agent experiences the outcome of all  $(N, K)$  codes in a single run. In this mode, we found that learning becomes much more efficient if we begin with a small range of configurations (e.g. 64) and gradually increase the range up to the maximum. Thus we employ a schedule that increase the number of configurations by 64 at regular intervals until it reaches the full range at about 50% of training.

### B.2. Multi-stage training

At  $N = 2048$ , we split the sequence into 4 segments and train each segment individually, while holding all previously learned segments fixed. This was needed to reduced the smoothing effect of averaging many rewards over the range of configurations considered.

## C. Runtime efficiency

After incorporating UPO and reducing graph connections to local context and actions, the main runtime bottleneck was reward generation. In the reference method (Liao et al., 2023), only a single configuration is learned in a single RL-training run, it requires generating a reward (running a BLER simulation) at every step within an episode. For a  $(128, 64)$  code, every episode takes 64 steps and around 10,000 episodes are used to train the model. This is only one single configuration.

By moving to universal sequence learning, we train all configurations jointly and each episode needed a single BLER simulation at termination. This reduced the BLER simulations requirement by orders of magnitude. Second, by running a multi-threaded multi-core CPU C++ Polar simulator implementation we achieved a 80x speed up compared to a standard Matlab implementation. We ran 16 environments in parallel at the largest sequence length thus producing another 16x speed up in training.

As an illustration, at  $N = 1024$ , we achieve 6 orders of magnitude improvement in runtime over the reference method using serial environment execution and standard Matlab based simulator.

### C.1. GPU-based Polar simulator implementation

We also evaluated the execution time for a data-parallel GPU-based implementation in Pytorch, with the initial belief that exploiting the SIMD architecture will lead to substantial runtime improvement. The simulator is configured to dispatch 1000 data blocks in parallel. However, the GPU implementation did not significantly improve over a single-core CPU C++ based implementation. We suspect that the simulator, which includes the encoder, noise generation and decoder, was sufficiently small that instruction and data are kept in cache for the entire C++ simulation run. We did not consider JIT compilation of the Pytorch implementation since we only had mixed successes with the feature and we do not expect it will provide the 7x improvement needed to match a 8-core C++ implementation.

## D. Training pipeline implementation

We document all software components used to facilitate implementation. The training pipeline is implemented in PyTorch<sup>3</sup> using the PyTorch Geometric (PyG)<sup>4</sup> library for graph machine learning and the PPO implementation from stable-baseline3<sup>5</sup>. Multi-node orchestration utilizes a custom dask<sup>6</sup>-based framework. The multi-threaded Polar decoder simulator is written in C++ using the native threading library with python/C++ interoperability handled via pybind11<sup>7</sup>.

<sup>3</sup><https://pytorch.org/>

<sup>4</sup><https://pytorch-geometric.readthedocs.io/>

<sup>5</sup><https://stable-baselines3.readthedocs.io/>

<sup>6</sup><https://www.dask.org/>

<sup>7</sup><https://pybind11.readthedocs.io/>